

Continuous Wave Two-Photon Scanning Near-Field Optical Microscopy

Achim K. Kirsch, Vinod Subramaniam, George Striker, Christoph Schnetter, Donna J. Arndt-Jovin, and Thomas M. Jovin

Department of Molecular Biology, Max Planck Institute for Biophysical Chemistry, D-37077 Göttingen, Germany

ABSTRACT We have implemented continuous-wave two-photon excitation of near-UV absorbing fluorophores in a scanning near-field optical microscope (SNOM). The 647-nm emission of an Ar-Kr mixed gas laser was used to excite the UV-absorbing DNA dyes DAPI, the bisbenzimidazole Hoechst 33342, and ethidium bromide in a shared aperture SNOM with uncoated fiber tips. Polytene chromosomes of *Drosophila melanogaster* and the nuclei of 3T3 Balb/c cells labeled with these dyes were readily imaged. The fluorescence intensity showed the expected nonlinear (second order) dependence on the excitation power in the range of 8–180 mW. We measured the fluorescence intensity as a function of the tip-sample displacement in the direction normal to the sample surface in the single- and two-photon excitation modes (SPE, TPE). The fluorescence intensity decayed faster in TPE than in SPE.

INTRODUCTION

Fluorescent dyes are used extensively in the biomedical sciences because of the sensitivity and selectivity they provide in identifying cellular constituents. Probes can be attached to molecules or specific cell organelles both in vivo and in fixed samples by numerous techniques (Haugland, 1996), including the expression of luminescent proteins fused to targets of interest (see, for example, Gerdes and Kaether, 1996). Using fluorescence spectroscopy and microscopy techniques, it has been possible to detect dyes down to the single-molecule level, thereby mapping the distribution and functional status of macromolecules and other components mediating cellular processes.

The DNA probe 4',6-diamidino-2-phenylindole (DAPI) exhibits a ~20-fold increase in fluorescence quantum yield upon binding to AT sequences in double-stranded DNA (Barcellona et al., 1990; Kapuscinski, 1995). A similar effect is exhibited by the bisbenzimidazole class of dyes, including Hoechst 33342 (BBI-342), which is taken up by living cells (Arndt-Jovin and Jovin, 1977). Probes not only enable the visualization of their target molecules, but also often reflect their environment via characteristic spectral or other photophysical changes, thus reporting on conditions such as acidity, polarity of the solvent, and the presence of specific ligands.

The excitation spectrum of biologically relevant dyes extends from the near-UV to the near-IR. However, dyes with absorption maxima in the UV (or near-UV), including DAPI and BBI-342, present problems for laser scanning microscopy. High-energy UV light is generally scattered and absorbed strongly by biological tissue, creating a deterioration of image quality and inducing photodamage of

living cells. Other major problems include the lack of inexpensive UV laser sources and the difficulty of producing UV-transmissive optics and objectives suitable for high-resolution imaging.

One solution to these problems is to use a process predicted in 1931 by Maria Göppert-Mayer: two-photon excitation (TPE), in which a molecule simultaneously absorbs two photons in a single quantum event. The combined energy of the two photons allows the use of irradiation in the visible (red) spectrum to excite UV dyes. The emission induced by this nonlinear excitation process is indistinguishable from the characteristic fluorescence in single-photon excitation (SPE) (Curley et al., 1992; Xu and Webb, 1996). TPE-based fluorescence microscopy has found widespread use since its introduction in 1990 (Denk et al., 1990, 1995; Bennett et al., 1996; König et al., 1996; Potter et al., 1996; Summers et al., 1996; Köhler et al., 1997; Masters et al., 1997; Svoboda et al., 1997). In addition to circumventing the technological problems of UV excitation in the microscope, TPE achieves 3D resolution without confocal (pinhole) detection, and at the same time suppresses photobleaching and the generation of fluorescence background outside the focal plane. These circumstances reflect the quadratic dependence of the excitation, restricting the probe volume to a small region around the focus.

A further consequence of the second-order nonlinearity of TPE is that the emitted mean fluorescence is proportional to the time-averaged square of the excitation intensity I . For continuous wave (cw) lasers this quantity is equal to the square of the average intensity. For an ideal laser source with square pulses of length τ and a repetition frequency f , one obtains an additional factor of $1/(\tau f)$ (Hänninen et al., 1994). For example, a typical femtosecond Ti:sapphire laser system ($\tau = 250$ fs, $f = 80$ MHz) provides a boost factor of 5×10^4 . This feature has led to the general use of femtosecond pulsed laser systems for TPE laser scanning microscopy (Denk et al., 1990; Curley et al., 1992; Wokosin et al., 1996).

Received for publication 9 March 1998 and in final form 14 May 1998.

Address reprint requests to Dr. Thomas M. Jovin, Department of Molecular Biology, Max Planck Institute for Biophysical Chemistry, Am Fassberg 11, D-37077 Göttingen, Germany. Tel.: 49-551-201-1381; Fax: 49-551-201-1467; E-mail: tjovin@mpc186.mpiibpc.gwdg.de.

© 1998 by the Biophysical Society

0006-3495/98/09/1513/09 \$2.00

In pulsed-TPE microscopy, saturation, bleaching, heating, optical trapping, and nonlinear optical effects arising from the high peak powers limit the average intensity in practice to a few milliwatts. However, TPE-laser scanning microscopy can also be implemented with cw lasers, which are in general cheaper and more readily available than femtosecond pulsed devices (Hänninen et al., 1994; Booth and Hell, 1998). To achieve signal levels similar to those attained with pulsed lasers, the time-averaged cw intensity has to be increased over the average intensity in the pulsed case by the factor $\sqrt{1/(\tau f)}$, leading to an average excitation intensity of several hundred milliwatts, which can be delivered easily by many cw-laser systems. The peak power is decreased by the same factor, thus shifting the potential limitations of the TPE technique from nonlinear to linear phenomena (Schönle and Hell, 1998).

In this contribution we report the use of cw-TPE in scanning near-field optical microscopy (SNOM). Near-field optical microscopes achieve their resolution by detecting the optical interaction between a nanometer-sized probe and the sample surface (Paesler and van Hulst, 1995). In most current SNOM designs, optical fibers are used to optically couple the interaction region to a light source (laser) and/or a detector. In addition to the usual problems with UV excitation mentioned above, optical fibers have a strong UV-excited autofluorescence that obscures the weak signals originating from the interaction region. Therefore, TPE offers major advantages for SNOM, particularly in the shared aperture mode of operation.

The experimental setup and techniques are presented in the next section, followed by images of various samples demonstrating the capabilities of the microscope. Power curves confirmed the nonlinear character of the excitation. In addition, the anticipated superior confinement of the TPE excitation in the SNOM, similar to that achieved in far-field TPE laser scanning microscopy, was established by recording z scans.

MATERIALS AND METHODS

Dyes

DAPI was purchased from Serva (Heidelberg, Germany), ethidium bromide (EtBr) from Sigma (Deisenhofen, Germany), Hoechst 33342 (BBI-342) from Calbiochem (Bad Soden, Germany), and TO-PRO-3 from Molecular Probes (Leiden, the Netherlands).

Polytene chromosomes

Polytene chromosome squashes were prepared from third-instar larvae salivary glands of *Drosophila melanogaster* according to an established protocol (Ashburner, 1989). The squashed chromosomes were washed in 100% ethanol and exchanged into phosphate-buffered saline (PBS) through an ethanol series (10 min each). Chromosomes were stained for 15 min at room temperature with 2 μ M DAPI, 5 μ M BBI-342, 10 μ M EtBr, or 2 μ M TO-PRO-3 in PBS. After they were rinsed twice with PBS, they were exchanged into ethanol through a gradient series, air dried, and stored in a desiccator. In some cases the chromosomes were kept hydrated after staining, and the samples were measured in the presence of a water film.

Cell samples

Mouse fibroblast cells (3T3 Balb/c) were grown on glass coverslips (12 mm) in Dulbecco's modified Eagle medium (all materials from Life Technologies, Eggenstein, Germany) containing 10% fetal calf serum. The coverslips were rinsed twice with cold PBS to remove the culture medium and fixed in MeOH at -20°C . The cells were rehydrated through a methanol series with PBS and permeabilized with 0.1% Triton X-100 in PBS for 5 min, followed by washing in PBS. They were incubated in 20 μ M BBI-342 in PBS for 15 min at room temperature. Coverslips were rinsed twice with PBS and dehydrated through an ethanol series, air dried, and stored in a desiccator.

SNOM

Our SNOM uses uncoated fiber tips for both excitation and detection of the fluorescence (shared aperture mode; Courjon et al., 1990; Bielefeldt et al., 1994; Kirsch et al., 1996). The tips were produced with a commercial pipette puller (P-2000; Sutter Instruments, Novato, CA) from a 9- μ m core diameter optical fiber (SMF 1528 CPC6; Siecor, Neustadt, Germany) and mounted in a shear-force sensor head developed in our laboratory for use with a commercial NanoScope IIIa SPM system (Digital Instruments, Santa Barbara, CA) (Kirsch et al., 1997, 1998). A conservative estimate of the resolution of the fiber probes used in this study was ~ 150 nm. When used to image 120-nm-diameter spherical fluorescent beads, the tips yielded apparent diameters of ~ 220 nm. The samples were scanned beneath the fiber tip in constant shear-force mode. Standard plane-fit and flattening corrections were applied to the data with the NanoScope software.

The 647-nm line of a Performa Ar-Kr mixed gas laser (Spectra Physics, Mountain View, CA) was long-pass filtered with an RG630 glass filter (Jenaer Glaswerk Schott and Gen., Mainz, Germany) and stabilized with an LS-PRO HP noise eater (Cambridge Research and Instrumentation, Cambridge, MA). The laser intensity was determined by the set point of the feedback loop of the LS-PRO noise eater. This set point can be externally controlled, and the output ranged from 8% to 78% of the input laser intensity. For SPE of TO-PRO-3 fluorescence, an additional 630DF30 excitation filter (Omega Optical, Brattleboro, VT) was used. The excitation light either passed through a dichroic mirror (505 DRLP; Omega) or was reflected by a beam splitter (Spindler and Hoyer, Göttingen, Germany) in the TPE and SPE modes, respectively. The dichroic was a standard filter for fluorescence microscopy, used in TPE in a slightly different geometry because the fluorescence is at a shorter wavelength than the excitation (Fig. 1 *a*). Particular attention was paid to the position of the reflective surface of the dichroic. For SPE the reflective surface faced the light source, whereas for TPE it faced the detector, thus avoiding the necessity of passing emission twice through the substrate material of the dichroic mirror. The excitation light was coupled to the 9- μ m fiber bearing the sensing tip on the far end, and fluorescence collected by this probe either was reflected by (TPE mode) or traversed (SPE mode) the dichroic mirror. Residual excitation light was removed by a suitable combination of detection filters: IF 395–547 and BG39 combined with an SWP490 or SWP560 (TPE), or 700 EFLP (SPE). The sources of these filters were Delta Light and Optics (Lyngby, Denmark) for SWP490, SWP560, Schott for IF 395–547 and BG39, and Omega for 700 EFLP. The fluorescence was detected by a single photon-counting avalanche photodiode (SPCM-AQ131; EG&G Optoelectronics, Vaudreuil, Quebec, Canada). For imaging, the TTL pulses generated by the APD were recorded by the pulse counting board of the NanoScope electronics.

Fluorescence-power curves were measured by automatically ramping the laser intensity up and down with the noise eater and simultaneously recording the fluorescence intensity detected by the APD with an external photon counter (SR400; Stanford Research Systems, Sunnyvale, CA). The noise eater was under computer control via the auxiliary ADCs and DACs of the lock-in amplifier used for shear-force detection (SR830; Stanford Research Systems). The fluorescence-power curves for the stained samples were recorded with the tip in shear-force feedback and zero scan size.

z scans were performed by bringing the tip from ~ 3 μ m above the sample surface into feedback control while recording the fluorescence. The

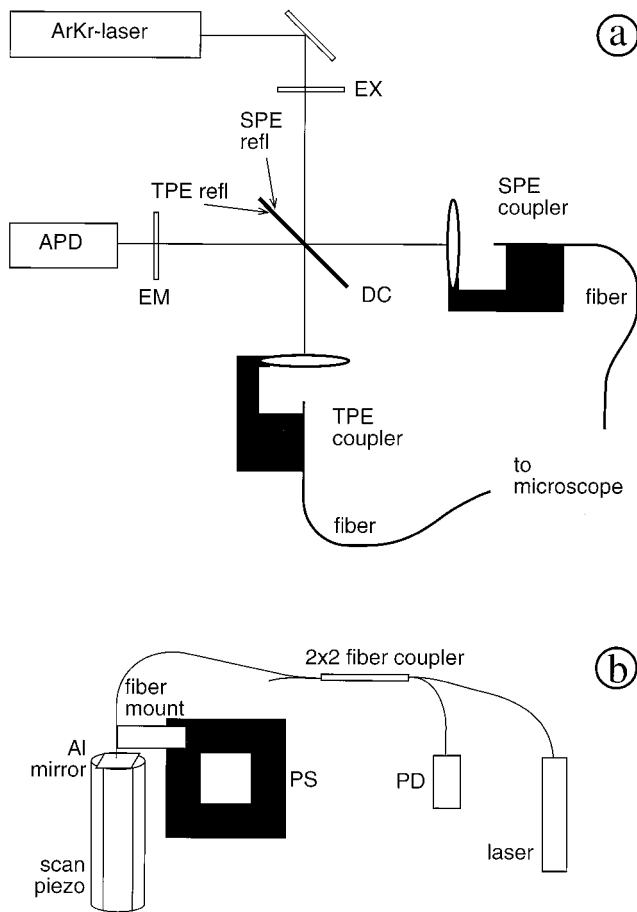


FIGURE 1 Optical configurations in TPE and SPE SNOM. (a) Optical setup for the use of a standard long-pass dichroic (DC) for single- and two-photon excitation SNOM. EX, excitation filter; EM, emission filter; APD, avalanche photo diode. SPE refl and TPE refl indicate the positions of the reflective side of the dichroic for SPE and TPE, respectively. SPE coupler and TPE coupler, beam-to-fiber coupler used for SPE and TPE, respectively. (b) Setup of the interferometer used to couple the calibrated piezo system (PS) to the scan piezo for calibration. PD, photo diode for detection of the interference.

z axis of the scan piezo was calibrated in a separate measurement against a piezo system with capacitive sensors and closed-loop position control (P-730.20; Physik Instrumente, Waldbronn, Germany). The calibrated piezo was coupled to the z axis of the scan piezo by phase-locking to an interferometer, formed by an Al mirror as the sample and the end face of a fiber mounted on the calibrated piezo (Fig. 1 b).

All measurements were performed under ambient conditions (relative humidity 45–60%, 18–24°C).

Data fitting procedures

Fluorescence-excitation intensity curves

Each experiment produced a number m (generally 10–40) of sweeps with increasing and decreasing illumination. During each sweep n points (generally 100–250) were collected by single photon counting. The analysis takes into account the fact that bleaching reduces the intensity of the fluorescence response in sequential sweeps. Because of the high noise level of the individual measurements, the m points (from m sweeps) for a given illumination level did not allow a determination of the bleaching factor. However, as the relative bleaching was presumed to be the same for all n

points, we fit the data simultaneously; i.e., for each of the n points we determined the error from $F_n = F_{0,n} \cdot \exp(-i/\tau)$ for sweeps $i = 0, \dots, m - 1$. These errors were summed over all of the points and minimized against τ . The resulting $F_{0,n}$ were then used as measured values for the n points, which were then fit either by the power function (Eq. 1) or by the second-order polynomial (Eq. 2; see Results and Discussion).

Fluorescence-distance curves

Each experiment produced a number of approach curves with decreasing distance between probe and sample surface. In each approach curve n points (generally 160–400) were collected by single-photon counting. As before, bleaching reduced the fluorescence intensity in successive approaches. Assuming a constant distance dependence, all curves were fit simultaneously to a double-exponential function with global decay lengths (Eq. 3; Results and Discussion).

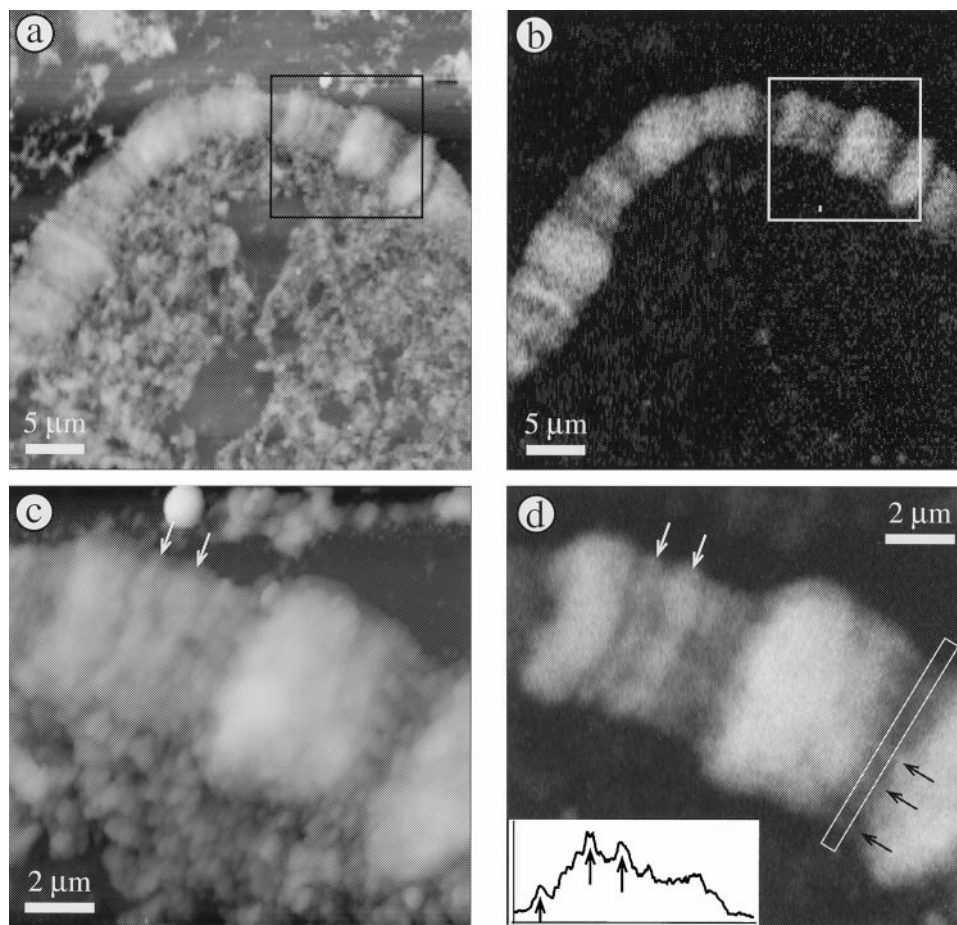
RESULTS AND DISCUSSION

cw-TPE imaging

The topography and simultaneously recorded cw-TPE fluorescence from a sample of DAPI stained polytene chromosomes of *Drosophila melanogaster* are shown in Fig. 2. The topographic images (Fig. 2, a and c) reveal that the DNA was surrounded by the remains of the salivary gland after squashing. These structures were absent from the fluorescence images (Fig. 2, b and d) because the enhancement of DAPI fluorescence only occurs when the dye is bound to double-stranded DNA. The chromosomes were ~50–270 nm in height, and cellular debris was in the range of ~150 nm. In general, the height variations along the longitudinal axis of the chromosome were similar to the fluorescence banding patterns, which is as expected, because height (mass) and total DNA content should be correlated. The topography and fluorescence of the region marked in Fig. 2, a and b, were recorded at higher magnification (Fig. 2, c and d). In the topography image, the material surrounding the chromosome exhibited many protrusions, the smallest having a width of ~150 nm. At this high resolution, the banding pattern of the chromosome showed differences between the topography and fluorescence images (*white arrows* in Fig. 2, c and d; note that the bands have similar heights but exhibit dramatically different fluorescence intensity), as is expected from the preference of the dye for AT tracks. In addition, chromatin fibers could be clearly seen along the chromosome axis in the interband region (*black arrows* in Fig. 2 d). From the average cross section (*inset* of Fig. 2 d) taken from the indicated rectangle, a width of ~360 nm for the brightest fiber was determined.

In images of cw-TPE fluorescence and shear-force topography, some bands showed inverted signals from the two contrast mechanisms, as demonstrated in Fig. 3, which depicts chromosome samples stained with DAPI. Most structures in these images were in register, with the exception of the band marked by the arrow in the lower left corner. In this case a higher band in the topography corresponded to a pronounced decrease in fluorescence intensity, as is seen more clearly in the line traces in Fig. 3 c, which

FIGURE 2 cw-TPE SNOM images of *Drosophila melanogaster* polytene chromosomes labeled with DAPI. (a) Topography and (b) fluorescence of a 39.22 μm square area. Scan parameters: 5 s per line, 256 points, 4.1 ms counting time/pixel; excitation: 31 mW at 647 nm, maximum counts per pixel = 25. (c) Topography and (d) fluorescence of the 13.25 μm square zoom marked in a and b. Scan parameters: 2.5 s per line, 256 points, 4.1 ms counting time/pixel; excitation: 92 mW at 647 nm, maximum counts per pixel = 226. The white arrows in c and d point to bands of similar height but different fluorescence intensity. The inset in d shows the average cross section taken from the white rectangle. The black arrows point to chromatin fibers.



were taken along the dashed lines in Fig. 3, a and b. The band with the inverted contrast is in the shaded region denoted I. The inversion was not caused by an offset between the optical and the topographical probes, as seen from the structures in the shaded region (II) that were in register. These images demonstrate clearly the different modes of contrast generation in stained polytene chromosomes. Whereas the fluorescence of DAPI originates preferentially from AT-rich regions, the topography depends only on the local mass density of chromatin and colocalized material independent of its composition. This consideration is essential in forming comparisons between band patterns obtained by optical and mechanical interactions.

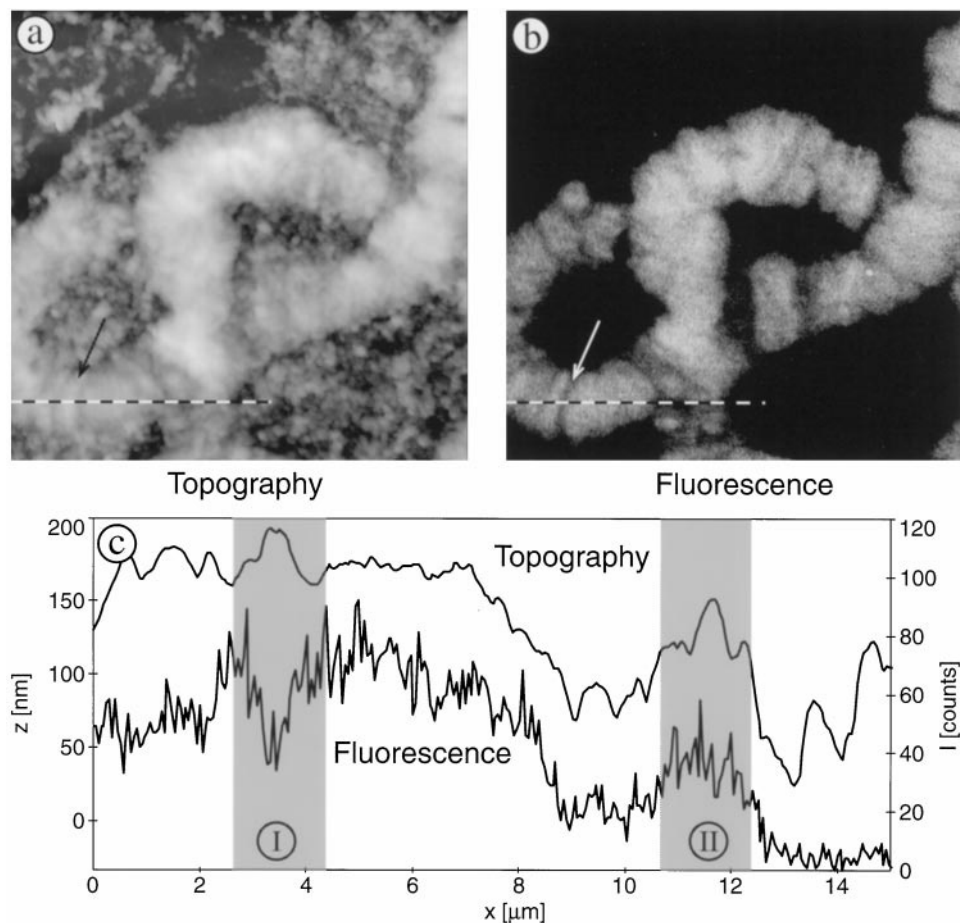
Structures within dried cells can also be imaged with cw-TPE fluorescence (Fig. 4, a and b). The DNA in the nucleus of fixed and dried 3T3 Balb/c cells was labeled with BBI-342. Because of the drying process the membranes collapsed and the nucleus became the dominant feature in both topographical and fluorescence images. The nucleoli were the highest features in the topography image, protruding ~ 220 – 300 nm above the mean surface of the nucleus, as seen previously in SFM images of similar material (Pitrasanta et al., 1994). The diameters were in the range of 2–12 μm . The fluorescence image, however, showed intensities uncorrelated to the topological signal. In these mouse cells BBI-342 stains predominantly the AT-rich centro-

mers within the nucleus, which are seen clustered around and over the nucleoli. However, the centromeres do not have more mass than the surrounding chromatin and thus were not distinguishable in the topological image. None of the cytoplasmic material around the nucleus that was clearly evident in the topological image fluoresced.

To assess the limits for TPE-SNOM imaging, we repeatedly scanned samples with increasing excitation intensity. The samples suddenly lost topographical contrast, and extremely bright streaks in the fluorescence channel appeared without any resemblance to the previously acquired fluorescence images. These observations corresponded to the physical depletion of the sample in the scan area. When the measurement was terminated at the first signs of degradation of the sample, stable topographical images could be restored only by drastically reducing the excitation intensity. However, the corresponding TPE fluorescence was no longer detectable. Sample degradation was independent of sample type and of the nature of the near-UV fluorophore.

As long as the samples lacked strong single-photon absorption at the excitation wavelength of 647 nm, we generally found no correlation between sample stability and the presence of a hydrating film or of the UV-absorbing dye. Our observations suggest that the degradation was not caused primarily by thermal effects, but rather was derived from chemical processes such as the creation of free radi-

FIGURE 3 cw-TPE SNOM of *Drosophila melanogaster* polytene chromosomes labeled with DAPI. (a) Topography and (b) fluorescence of a 26.3 μm square area. Scan parameters: 3.3 s per line, 512 points, 3.1 ms counting time/pixel; excitation: 68 mW at 647 nm, maximum counts per pixel = 141. (c) Topography (upper trace) and fluorescence (lower trace) along the dashed line in a and b. In the shaded region I, the correlation between fluorescence and topography is inverted with respect to that in region II.



calcs. We attempted dual-mode (SPE and TPE) imaging with samples doubly labeled with a near-UV absorbing fluorophore and TO-PRO-3, which has a peak absorption at 642 nm. SPE imaging was routinely achieved, but these specimens were too sensitive for TPE imaging, likely because of thermal effects from single photon absorption at high light levels and chemical damage such as photocleavage of the DNA under the intense illumination (Åkerman and Tuite, 1996).

In contrast to dried cells, SNOM imaging of live cells is considerably more challenging. Although far-field cw-TPE imaging of living cells in a confocal microscope has been readily demonstrated (Hell et al., manuscript submitted for publication), the shear-force feedback system in our cw-TPE SNOM has yet to be adapted for operation in solution. We note, however, that the mechanism has been demonstrated to function under water (Moyer and Kammer, 1996; Brunner et al., 1997; Mertesdorf et al., 1997; Gheber et al., 1998; Lambelet et al., 1998). The scan speed of the SNOM would have to be increased to minimize disturbances originating from the movements of living cells. Finally, the characteristics of the optical probe have to be modified for operation in liquid, inasmuch as the light confinement effect strongly depends on the refractive index difference between the glass of the fiber and the surrounding medium. This difference is much larger for the glass-air than for the glass-water interface.

Excitation-power/fluorescence intensity curves

The dependence of the fluorescence intensity on the excitation power is shown in Fig. 5. In Fig. 5, a, b, and c, the fiber tip was in shear-force contact with polytene chromosome samples labeled with DAPI, BBI-342, and EtBr, respectively. For comparison, Fig. 5 d shows the same experiment for a bare uncoated fiber tip. The power curves were fit to the function

$$F = d \cdot I^e + f \quad (1)$$

where I is the excitation intensity, d is the amplitude, e is the order of the excitation, and f is the dark count rate of the detector and experiment independent light. For linear relationships, as in conventional SPE, e should be 1, whereas for a pure two-photon absorption process the exponent should be 2. This functional dependence (Eq. 1) has been used in many other reports of TPE (Denk et al., 1990; Curley et al., 1992; Xu and Webb, 1996). We summarize the parameter e for our experiments in Table 1. We find that for the labeled biological samples the exponents were very close to 2, in agreement with the interpretation of our data in terms of a two-photon excitation process.

For the optical fiber the exponent was clearly <2 , indicative of a superimposed linear contribution to the TPE optical signal. Although previous observations (Meiners,

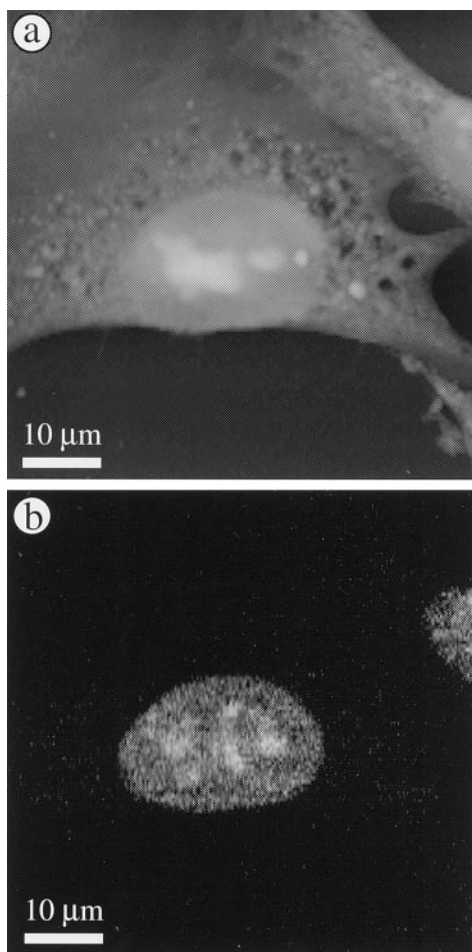


FIGURE 4 cw-TPE SNOM images of 3T3 Balb/c cells labeled with BBI-342. (a) Topography and (b) fluorescence of a 60 μm square area. Scan parameter: 4.3 s per line, 256 points, 4.1 ms counting time/pixel; excitation: 90 mW at 647 nm, maximum counts/pixel = 27. The protrusions in the topography image are nucleoli, and the brighter spots in the fluorescence image surrounding them are the AT-rich centromeres.

1997) suggest that the polymeric coating protecting optical fibers is a source of strong UV-excited fluorescence, we do not expect this to have been a major contribution in our case. We would rather attribute the intrinsic fiber fluorescence to impurities in the fiber core and cladding. Although the density of these impurities is probably low, the length of the fiber (~ 70 cm) can lead to a detectable integrated signal.

To account for both linear and nonlinear contributions to the fluorescence signal, a second-order polynomial was fit to the data (instead of the power function of Eq. 1):

$$F = a + bI + cI^2 \quad (2)$$

where I is the excitation intensity, a is the background signal, bI is the linear contribution including excitation light leaking to the detector, and cI^2 is the second-order nonlinear processes. Permitting both a linear term and a free exponent would lead to an overinterpretation of the data. Fig. 5 shows data corrected for bleaching (see Materials and Methods) and the best fit to the polynomial function. The quality of

the fits can be assessed by the normalized residuals and their autocorrelation. In the excitation power range accessible in our experimental setup, the difference between the fits to our data of Eqs. 1 and 2 was smaller than the Poisson noise envelope given by the photon statistics. Thus a preferred function could not be identified.

The contributions of the three terms a , bI , and cI^2 of Eq. 2 to the fit for an excitation intensity of 100 mW are given in Table 1. As expected from the low exponent of the power function (Eq. 1), we found comparable contributions of the linear and the quadratic terms to the optical signal of the bare optical fiber. In contrast, in the case of the stained samples, the nonlinear term dominated the fluorescence signal, as indicated by an exponent very close to 2 in the power function. It has to be emphasized that although the qualitative behavior of the fluorescence in these experiments was similar, the absolute count rates were not comparable because of the different probes, dye concentrations, and filter combinations.

In the simple model based on a second-order polynomial (Eq. 2), contributions from some processes are not included, which could also account for the small negative count rate in the offset for the DAPI-stained sample (Table 1). Possible effects include:

Bleaching. We compensated for bleaching partly by alternating the direction in which the power curves were taken, and by the simultaneous global analysis of the data. However, the assumption of a linear time course for bleaching may have been inadequate in some cases.

Temperature dependence of fluorescence quantum yield. Assuming an inverse linear dependence of the emission on the sample temperature, this effect would lead to a third-order dependence with a negative coefficient of the TPE fluorescence on the excitation power. Such an effect would contribute to the first-order term in the polynomial function (Eq. 2) or to an exponent of <2 in the exponential analysis (Eq. 1).

Other higher order nonlinear effects. For example, three-photon absorption would lead to a cubic term in the excitation intensity in the polynomial.

z distance/fluorescence intensity curves

For confocal microscopy TPE offers an inherent 3D resolving power without the use of a pinhole in front of the detector (Denk et al., 1990). The corresponding phenomenon in near-field optical microscopy is shown in Fig. 6, as are the different photobleaching behaviors. The dependence of the fluorescence intensity on the distance between the sample surface and the probe for TPE of DAPI and SPE of TO-PRO-3 is given in Fig. 6, *a* and *b*, respectively. The dyes were bound to polytene chromosomes. In Fig. 6 *a*, 13 approach curves are overlaid to emphasize the lack of photobleaching effects, whereas in Fig. 6 *b* the first, third,

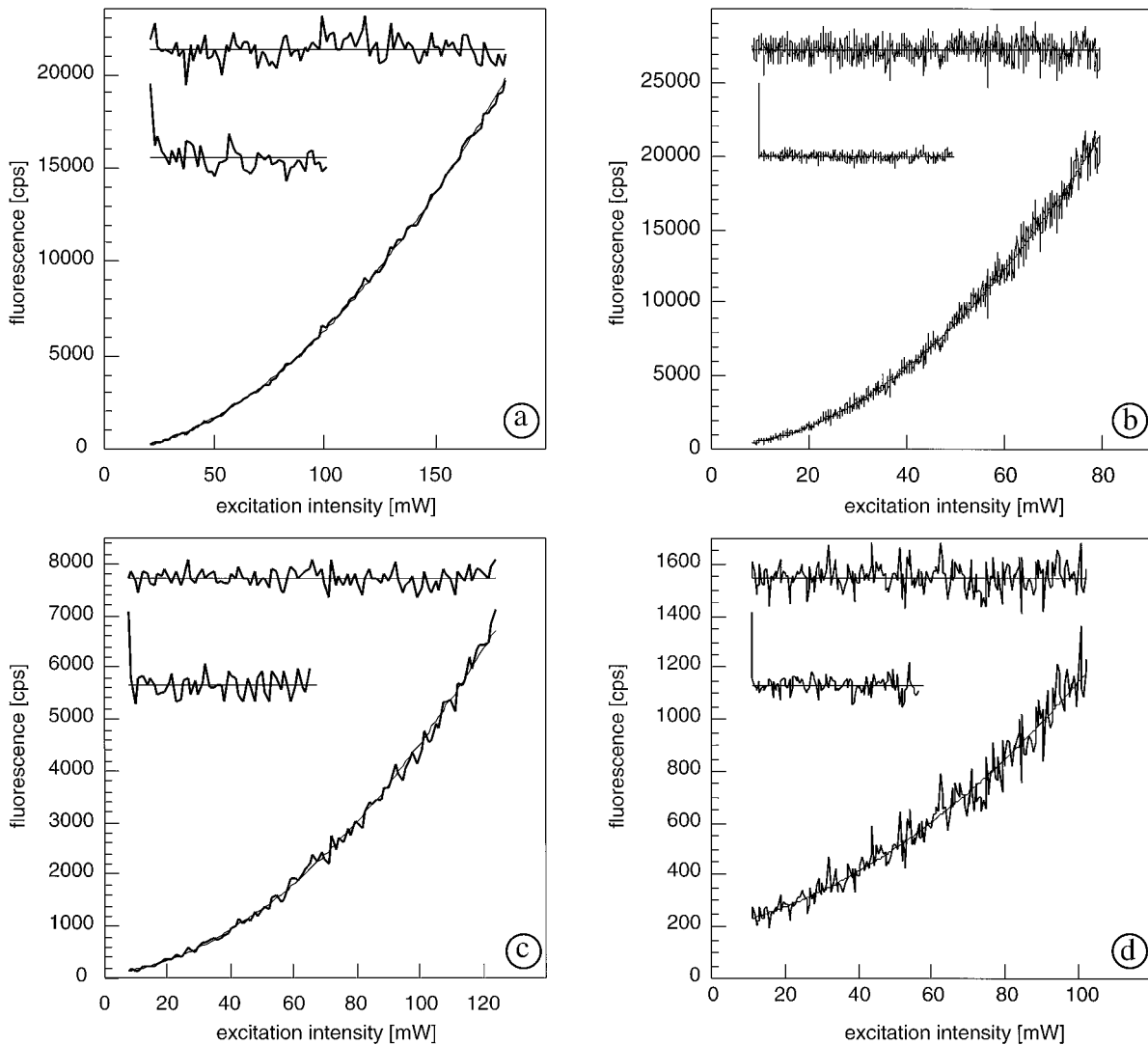


FIGURE 5 Power curves measured on polytene chromosomes labeled with (a) DAPI, (b) BBI-342, (c) EtBr. (d) Power curve for a bare fiber of typical length (70 cm). The data and the best fit to a second-order polynomial are shown (Eq. 2). The inset curves are weighted residuals (*upper*) and autocorrelations (*lower*). Fits to Eq. 1 (not shown) are of equal quality. For presentation purposes the ordinates have been scaled to counts per second (cps). Counting time: 0.1 s for *a*, *c*, and *d* and 0.02 s for *b*.

and ninth approaches are depicted, exhibiting clear photobleaching. The solid lines are fits to a double exponential,

$$F_i = g_i \cdot e^{-z/z_1} + h_i \cdot e^{-z/z_2} + k_i \quad (3)$$

where F_i is the fluorescence of approach i ; z_0 and z_1 represent the global apparent decay lengths of an experiment; and g_i , h_i , and k_i are the amplitudes and offset for approach i .

The double exponential was used to parameterize the overall dependence of the fluorescence on the distance between the fiber probe and the sample, inasmuch as it led to an accurate fit within the limits dictated by the noise envelope; a single exponential failed to describe the data adequately. The decay lengths from the fits are given in Table 2. They were much smaller for the TPE of DAPI than

TABLE 1 Results of the fits to the power curves for different dyes and the bare fiber

Dye	a	bl	cI^2	e	$\langle e \rangle$
DAPI	-27	118	543	1.9	1.88 ± 0.18
BBI-342	25	20	3360	2.0	1.92 ± 0.09
EtBr	6	65	381	1.9	1.91 ± 0.02
bare fiber	19	27	58	1.7	1.76 ± 0.12

a , bl , and cI^2 , count rates for 0.1 s with 100 mW excitation power; fits of Eq. 2 were made to the data in Fig. 5. e , the exponent from fits of the same data to Eq. 1; $\langle e \rangle$, mean value for all experiments.

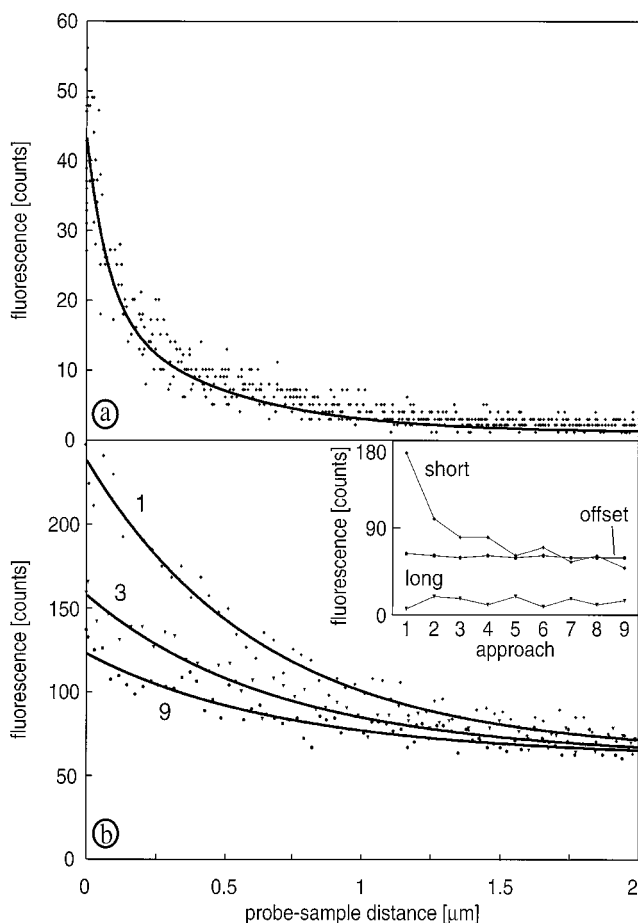


FIGURE 6 Fluorescence-distance curves taken over polytene chromosomes labeled with (a) DAPI or (b) TO-PRO-3. (a) Thirteen individual sample approaches and a double-exponential fit. Excitation: 179 mW at 647 nm. (b) First, third, and ninth approach and double exponential fits with global decay lengths. Excitation: 5.1 μ W at 647 nm. The inset shows the amplitudes of the components with short and long decay lengths and the offset. Counting time per data point, 4.1 ms.

for the SPE of TO-PRO-3 fluorescence. That is, the thickness of the surface layer contributing to the fluorescence signal is much smaller in the case of TPE than with SPE. This result has profound implications for the potential uses of TPE-SNOM.

The double-exponential fit also allowed a more detailed analysis of the bleaching in these curves. Whereas no bleaching was observed in TPE of DAPI, the SPE TO-PRO-3 signal decreased dramatically within the first approaches (Fig. 6 b). The individual amplitudes g_i , h_i , and k_i

TABLE 2 Decay lengths of the fluorescence-distance curves

Dye	z_0	z_1
DAPI	75 nm	447 nm
TO-PRO-3	626 nm	1726 nm

z_0 and z_1 , the decay lengths obtained from the simultaneous fit of the approach curves to a double-exponential function (Eq. 3), with varying amplitudes for the individual approaches.

of the three components are plotted in the inset to Fig. 6 b. Only the component with the short decay length faded away, while the long decay length component and the offset remained approximately constant. We conclude that the fluorescence contributing to the individual terms of the double-exponential curve originated from different physical processes with differential susceptibilities to bleaching.

The background signal levels in the two experiments were also different. For TPE the background level was 1.6 counts/4.1 ms dwell time compared to 61 counts/4.1 ms for SPE. Although the signal levels cannot be compared because of the different filter sets, dyes, and dye concentrations used, it was generally observed that the signal background in TPE experiments was much smaller than for SPE fluorescence. This difference was probably due to fiber fluorescence and Raman scattering in the latter case.

CONCLUSIONS

We have demonstrated that continuous-wave two-photon excitation is feasible in a shared aperture scanning near-field optical microscope (cw-TPE-SNOM). This mode extends the accessible spectral range to the near-UV and offers dramatically improved signal-to-noise ratios. Furthermore, the thickness of the surface layer contributing to the optical signal is reduced significantly. Although not yet demonstrated, an improved lateral resolution can be anticipated, owing to the quadratic dependence of the fluorescence on the local excitation intensity.

We thank S. W. Hell for motivating discussions.

VS was supported by a long-term fellowship from the Human Frontiers Science Program Organisation.

REFERENCES

- Åkerman, B., and E. Tuite. 1996. Single- and double-strand photocleavage of DNA by YO, YOYO and TOTO. *Nucleic Acids Res.* 24:1080–1090.
- Arndt-Jovin, D. J., and T. M. Jovin. 1977. Analysis and sorting of living cells according to deoxyribonucleic acid content. *J. Histochem. Cytochem.* 25:585–589.
- Ashburner, M. 1989. Salivary gland chromosome squash technique: simple method. *In Drosophila, A Laboratory Manual.* Cold Spring Harbor Laboratory, Cold Spring Harbor, NY. 28–29.
- Barcellona, M. L., G. Cardiel, and E. Gratton. 1990. Time-resolved fluorescence of DAPI in solution and bound to polydeoxynucleotides. *Biochem. Biophys. Res. Commun.* 170:270–280.
- Bennett, B. D., T. L. Jetton, G. Ying, M. A. Magnuson, and D. W. Piston. 1996. Quantitative subcellular imaging of glucose metabolism within intact pancreatic islets. *J. Biol. Chem.* 271:3647–3651.
- Bielefeldt, H., I. Hörsch, G. Krausch, M. Lux-Steiner, J. Mlynek, and O. Marti. 1994. Reflection-scanning near-field optical microscopy and spectroscopy of opaque samples. *Appl. Phys. A.* 59:103–108.
- Booth, M. J., and S. W. Hell. 1998. Continuous wave excitation two-photon fluorescence microscopy exemplified with the 647 nm ArKr laser line. *J. Microsc.* 190:298–304.
- Brunner, R., A. Bietsch, O. Hollricher, and O. Marti. 1997. Distance control in near-field optical microscopy with piezoelectrical shear-force detection suitable for imaging in liquids. *Rev. Sci. Instrum.* 68:1769–1772.

- Courjon, D., J. M. Vigoureux, M. Spajer, K. Sarayeddine, and S. Leblanc. 1990. External and internal-reflection near-field microscopy—experiments and results. *Appl. Opt.* 29:3734–3740.
- Curley, P. F., A. I. Ferguson, J. G. White, and W. B. Amos. 1992. Application of a femtosecond self-sustaining mode-locked Ti:sapphire laser to the field of laser scanning confocal microscopy. *Opt. Quantum Electron.* 24:851–859.
- Denk, W., D. W. Piston, and W. W. Webb. 1995. Two-photon molecular excitation in laser-scanning microscopy. In *Handbook of Biological Confocal Microscopy*. Plenum Press, New York. 445–458.
- Denk, W., J. H. Strickler, and W. W. Webb. 1990. Two-photon laser scanning fluorescence microscopy. *Science*. 248:73–76.
- Gerdes, H. H., and C. Kaether. 1996. Green fluorescent protein: applications in cell biology. *FEBS Lett.* 389:44–47.
- Gheber, L. A., J. Hwang, and M. Edidin. 1998. Design and optimization of a near-field scanning optical microscope for imaging biological samples in liquid. *Applied Optics*. 37:3574–3581.
- Göppert-Mayer, M. 1931. Über Elementarakte mit zwei Quantensprüngen. *Ann. Phys.* 9:273–295.
- Hänninen, P. E., E. Soini, and S. W. Hell. 1994. Continuous wave excitation two-photon fluorescence microscopy. *J. Microsc.* 176:222–225.
- Haugland, R. P. 1996. *Handbook of Fluorescent Probes and Research Chemicals*. Molecular Probes, Eugene, OR.
- Kapuscinski, J. 1995. DAPI: a DNA-specific fluorescent probe. *Biotech. Histochem.* 70:220–233.
- Kirsch, A. K., C. K. Meyer, H. Huesmann, D. Möbius, and T. M. Jovin. 1998. Fluorescence SNOM of domain structures of LB films containing electron transfer systems. *Ultramicroscopy*. 71:295–302.
- Kirsch, A., C. Meyer, and T. M. Jovin. 1996. Integration of scanning probe microscopes with optical techniques. In *NATO Advanced Research Workshop: Analytical Use of Fluorescent Probes in Oncology*, Miami, FL. Plenum Press, New York. 317–323.
- Kirsch, A. K., C. K. Meyer, and T. M. Jovin. 1997. Shear force imaging of DNA in a near-field scanning optical microscope (NSOM). *J. Microsc.* 185:396–401.
- Köhler, R. H., J. Cao, W. R. Zipfel, W. W. Webb, and M. R. Hanson. 1997. Exchange of protein molecules through connections between higher plant plastids. *Science*. 276:2039–2042.
- König, K., U. Simon, and K. J. Halbhauer. 1996. 3D resolved two-photon fluorescence microscopy of living cells using a modified confocal laser scanning microscope. *Cell. Mol. Biol.* 42:1181–1194.
- Lambelet, P., M. Pfeffer, A. Sayah, and F. Marquis-Weible. 1998. Reduction of tip-sample interaction forces for scanning near-field optical microscopy in a liquid environment. *Ultramicroscopy*. 71:117–121.
- Masters, B. R., P. T. C. So, and E. Gratton. 1997. Multiphoton excitation fluorescence microscopy and spectroscopy of in vivo human skin. *Biophys. J.* 72:2405–2412.
- Meiners, J.-C. D. 1997. *Nanostrukturen in ultradünnen Blockcopolymerfilmen*. Hartung-Gorre Verlag, Konstanz, Germany.
- Mertesdorf, M., M. Schonhoff, F. Lohr, and S. Kirstein. 1997. Scanning near-field optical microscope designed for operation in liquids. *Surface Interface Anal.* 25:755–759.
- Moyer, P. J., and S. B. Kammer. 1996. High-resolution imaging using near-field scanning optical microscopy and shear force feedback in water. *Appl. Phys. Lett.* 68:3380–3382.
- Paesler, M., and N. F. van Hulst, editors. 1995. Near-field optics and related techniques. *Ultramicroscopy*. 61:1–311.
- Pietrasanta, L. I., A. Schaper, and T. M. Jovin. 1994. Imaging subcellular structures of rat mammary carcinoma cells by scanning force microscopy. *J. Cell. Sci.* 107:2427–2437.
- Potter, S. M., C. M. Wang, P. A. Garrity, and S. E. Fraser. 1996. Intravital imaging of green fluorescent protein using two-photon laser-scanning microscopy. *Gene*. 173:25–31.
- Schönle, A., and S. W. Hell. 1998. Heating by linear absorption in the focus of an objective lens. *Opt. Lett.* 23:325–327.
- Summers, R. G., D. W. Piston, K. M. Harris, and J. B. Morrill. 1996. The orientation of first cleavage in the sea urchin embryo, *Lytechinus variegatus*, does not specify the axes of bilateral symmetry. *Dev. Biol.* 175:177–183.
- Svoboda, K., W. Denk, D. Kleinfeld, and D. W. Tank. 1997. In vivo dendritic calcium dynamics in neocortical pyramidal neurons. *Nature*. 385:161–165.
- Wokosin, D. L., V. Centonze, J. G. White, D. Armstrong, G. Robertson, and A. I. Ferguson. 1996. All-solid-state ultrafast lasers facilitate multiphoton excitation fluorescence imaging. *IEEE J. Sel. Top. Quant. Elec.* 2:1051–1065.
- Xu, C., and W. W. Webb. 1996. Measurement of two-photon excitation cross sections of molecular fluorophores with data from 690 to 1050 nm. *J. Opt. Soc. Am. B.* 13:481–491.